Performance model for parabolic trough solar thermal power plants with thermal storage. Comparison to operating plant data.

Isabel Llorente García, José Luis Álvarez, Daniel Blanco

INITEC-Energía. Renewable Energy Dept. R&D. Vía de los Poblados, 11 - Edificio Trianón C. 28033, Madrid, Spain.

Abstract

This paper describes a simulation model that reproduces the performance of parabolic trough solar thermal power plants with a thermal storage system. The aim of this model is to facilitate the prediction of the electricity output of these plants during the various stages of their planning, design, construction and operation. Model results for a 50 MWe power plant are presented and compared to real data from an equivalent power plant currently operated by the ACS Industrial Group in Spain.

Keywords:
renewable energy, solar thermal, parabolic trough, thermal storage, performance model

1. Introduction

Solar power technology has seen great advances over the past decade. Both photovoltaic (PV) and concentrating solar power (CSP) technologies now constitute feasible commercial options for large scale power plants as well as for smaller electricity and heat generating devices. PV energy is based on the direct generation of an electric current from a material (typically a semiconductor) that exhibits the photovoltaic effect when exposed to sunlight (direct or diffuse). The principle of CSP (also referred to as solar thermal power), on the other hand, is the use of the heat generated by direct solar radiation concentrated onto a small area with the purpose of producing electricity.

There are currently four basic commercially available CSP technologies. Two of them, parabolic trough and Fresnel linear collectors, concentrate direct sunlight onto a line, whereas the other two, parabolic dish and solar tower technologies, concentrate light onto a point.

The use of CSP with practical purposes dates back to the second half of the 19^{th} century, when inventors such as the British William Adams, the French Augustin Mouchot, the Italian Alessandro Battaglia and the Swede John Ericsson demonstrated a number of solar energy devices such as solar cookers, water distillers, ice makers and boilers for steam engines, setting the basis for current CSP designs and even taking some first steps towards the development of energy storage (Bradford, 2006). In the beginning of the 20^{th} century, home solar water heaters were commercialised in South West USA and the North-American Frank Shuman successfully completed a parabolic trough plant for powering an irrigation system in Meadi, Egypt, in 1913. The Italian Giovanni Francia designed and built the first linear Fresnel collector in Genoa, Italy, in 1964 and the first solar tower plant in Sant'Ilario, Italy, in 1965. The *Solar One* tower was built in 1981 in California as a demonstration project with a capacity of 10 MW_e. The nine parabolic trough Solar Energy Generating Systems (SEGS), built between 1984 and 1990 in California, USA, remain the largest solar energy generating facility in the world today, with 354 MW_e of installed capacity. The world's first commercial solar tower, *PS10*, was finished in Seville, Spain, in 2007 and has a capacity of 11 MW_e.

From the available CSP technologies, parabolic trough is the most widespread today, with around 29 plants in operation and around 1220 MW_e of installed power in the world, corresponding to 96.3 % of the total operational concentrating solar power as of the beginning of 2011 (see Fig. 1). Most of these plants

Email addresses: isabel_llorente_garcia@hotmail.com (Isabel Llorente García), dblanco@initec-energia.com,dblanco75@gmail.com (Daniel Blanco)

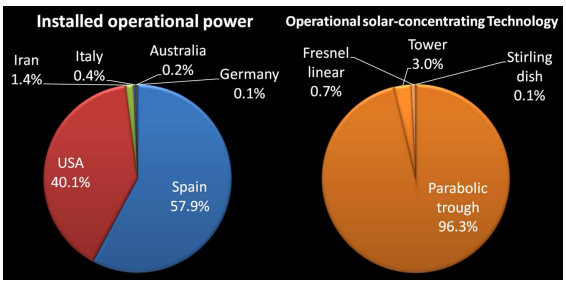

Figure 1: Solar thermal power plant projects in operation in the world (March 2011). **Left**: installed power by country. **Right**: installed power by technology.

are located in Spain and the USA, as shown in the same figure. With regard to projects under construction or announced, the proportion of tower, parabolic dish and Fresnel projects increases to approximately 28 %, and a number of countries such as Australia, France, Egypt, Algeria, Morocco, South Africa, Sudan, United Arab Emirates, Israel, India and China are embracing the development of solar thermal power plants in their territories.

This paper presents a detailed performance model for a parabolic trough plant with thermal energy storage (TES) together with a comparison of the model results to measured data from an operating plant of this type. This is the first published detailed comparison of simulation results to actual data from an operating plant with storage. The good agreement obtained validates the model and confirms it as an effective tool for predicting the electricity output of these plants.

Other performance models for parabolic trough CSP plants can be found in the literature. Full models for plants with no TES have been presented in Lippke (1995); Price et al. (1995); Patnode (2006); Jones et al. (2001) and have been validated against experimental data from a SEGS plant with no TES system. Price (2003) expands the work in Price et al. (1995) by including a TES system in the simulation. There are several documented complete models for trough plants with storage, namely: System Advisor Model (*SAM*) (Price, 2003; Blair et al., 2008b,a; Wagner et al., 2010; SAM, 2011) from the National Renewable Energy Laboratories in the USA (NREL), *Greenius* (Dersch et al., 2008; Hennecke et al., 2010; Greenius, 2011) from the German Aerospace Centre (DLR), *SOLERGY* (Stoddard et al., 1987) from Sandia National Laboratories in the USA (originally a model for tower plants, it has been updated over the years to accurately model trough plants (Kolb, 2011)) and the model in Montes et al. (2009). However, reports of detailed comparison to actual trough plant data are not easily found. More recent performance models for trough plants with no TES can be found in Rolim et al. (2009); Larrain et al. (2010). A comprehensive list of software tools for CSP performance modelling is presented in Ho (2008), while the quantification of uncertainties and sensitivities through probabilistic modelling is specifically addressed in Ho et al. (2011).

An effort towards the standardisation and benchmarking of solar thermal performance models is currently being made by the international community within the *SolarPACES guiSmo* project, which brings together experts from the DLR, NREL, Sandia National Laboratories, the Centre for Energy, Environmental and Technological Research in Spain (CIEMAT), the National Centre for Renewable Energy in Spain (CENER), etc., as well as several industrial partners.

The model presented in this paper was benchmarked within work package 9.2 of the *guiSmo* project, which focused on the modelling of a SEGS-VI-like trough plant without energy storage or fossil back-up. Relevant result variables for three representative weeks of a year were compared to those from 10 other models. Our results for total daily gross electric energy generated differ on average from those from DLR, Sandia National Laboratories and NREL by no more than 11%, 5% and 2%, respectively (further details available on request).

2. Parabolic trough power plant with thermal storage

A simplified schematic for a parabolic trough solar thermal power plant with thermal storage is shown in Fig. 2. These plants typically consist of three main circuits: the Solar Field, through which the heat transfer fluid (HTF) circulates, the Power Block, which circulates water and steam, and the TES system. The HTF and water-steam circuits and the HTF and TES circuits can exchange energy at the corresponding heat exchangers.

The Solar Field consists of a number of parabolic trough collector loops connected in parallel to each other. Each loop consists of several solar collector assemblies (SCA) in series, in one or several rows. Each SCA consists in turn of several solar collector elements (SCE). Each SCE is made of highly reflective parabolic mirrors with receiver tubes or heat collection elements (HCE) mounted at the focal line of the parabolic surface. The HTF is distributed to the loops in the Solar Field by means of insulated pipes. A single-axis

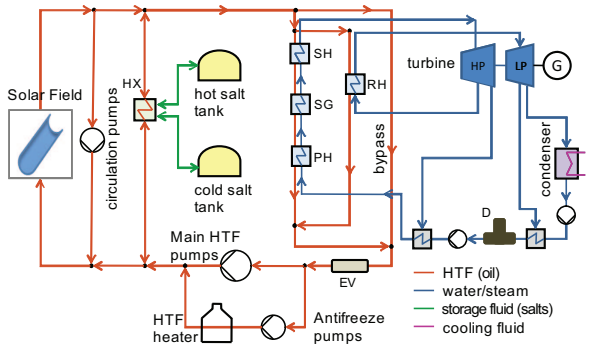

Figure 2: Schematic diagram of a parabolic trough solar thermal power plant with thermal storage. In the figure, HX stands for heat exchanger, PH, SG, SH and RH for preheater, steam generator, superheater and reheater, respectively, D stands for deaerator and EV for expansion vessel.

tracking mechanism allows the collectors to follow the sun from sunrise to sunset. Solar energy is reflected by the parabolic trough collector mirrors and concentrated onto the receiver tubes which absorb a high fraction of it, heating up the HTF that circulates in the Solar Field, which enters one end of the loops at a cold temperature and leaves hot through the other end after absorbing heat from the sun.

The Power Block consists of a heat exchanger train (preheaters, steam generators, superheaters and reheaters), a steam turbine and electricity generator, a condenser, a cooling system (cooling tower, air-cooler condenser, hybrid) and other auxiliary equipment. The thermal energy absorbed in the Solar Field is transferred to the water and steam in the Power Block in order to produce steam at high temperature and pressure, which enters the turbine, generating electricity. Steam leaving the turbine passes though the condenser, where it condenses and cools down, and is then circulated again towards the preheaters, closing the water-steam cycle.

Solar energy can be stored as sensible heat in the thermal storage medium during the hours of high insolation, while it is possible to extract that heat during the hours of low or zero insolation for the production of electricity. In this paper we will assume that the TES system is a two-tank molten-salt system. Storage of the absorbed energy in the salts reduces the dependence of the plant's performance on meteorological conditions and guarantees a higher and steadier electricity production on a daily basis.

A fossil fuel back-up system (e.g. natural gas) can assist the operation of the plant by allowing warm up of the HTF as required, for instance as a freeze-protection measure for the HTF.

3. Performance model

The simulation algorithm has been written and developed in *Wolfram*'s *Mathematica 7* software. The aim of the simulation is to allow detailed prediction and analysis of the plant's electricity production on a daily, monthly and yearly basis. The model intends to be a flexible tool and can be tailored to the specific characteristics of any trough plant of choice. The model can be very useful during the design stages of a project and can assist in the optimisation of the plant's operation strategy with a view to maximising the electricity generated.

3.1. Algorithm structure

Fig. 3 shows a simplified schematic with the general structure of the information flow within the simulation algorithm. Details of the calculations are given in the next section 3.2.

The box on the left hand side of the figure summarises the inputs required by the simulation. These include geographical and meteorological data for the plant's site and specifications for the different subsystems of the plant, i.e., the Solar Field, Power Block and TES system.

The algorithm uses the geographical and meteorological data and the Solar Field specifications to calculate the corresponding solar time and angle of incidence of the solar radiation on a collector operating on sun-tracking mode. These results together with calculations of the Solar Field efficiency (see section 3.2.5), HCE thermal losses (section 3.2.7) and Solar Field piping losses (section 3.2.8) are used to obtain the useful thermal power delivered by the Solar Field (section 3.2.10). The HTF temperature is calculated as detailed in section 3.2.9 and used together with the result for the useful thermal power from the Solar Field, the state of the storage tanks and the state of the turbine (on/off), to decide the plant's operating mode (see section 3.2.15) and calculate the corresponding thermal powers sent to the Power Block and to the TES system, or extracted from the TES system. Together with the technical specifications of the Power Block and other equipment, these results are then used to calculate the gross electric power generated, the plant's parasitic consumption and, finally, the net electricity production.

Fig. 4 shows a preview of the results generated by the performance model for a summer day. The graph shows the input solar irradiance and results for the useful thermal power delivered by the Solar Field, thermal

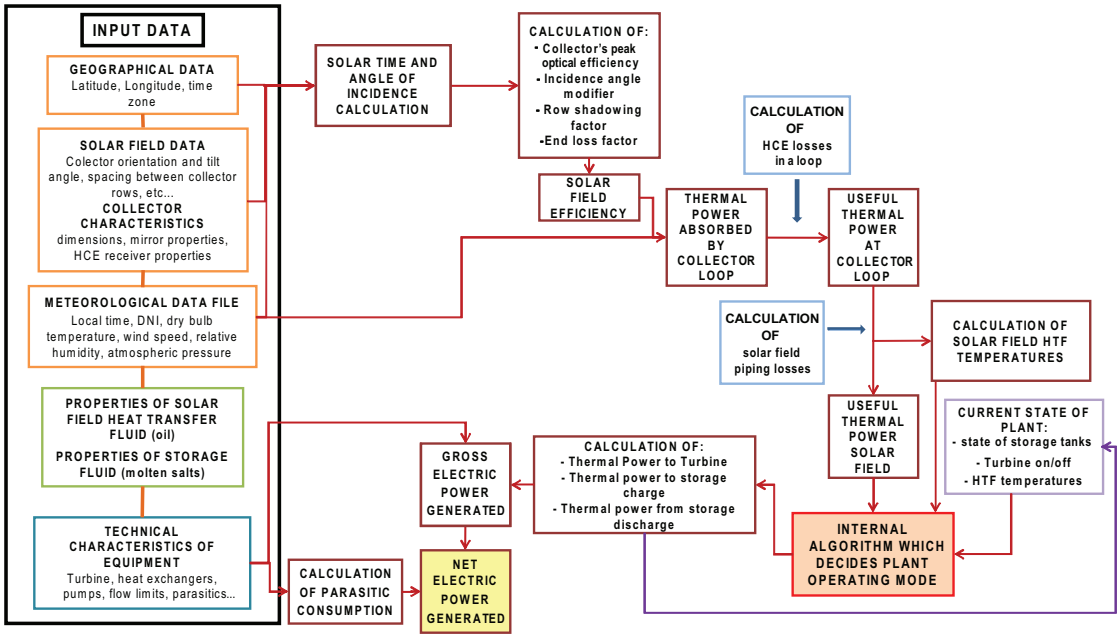

Figure 3: Schematic representation of the information flow within the performance model algorithm.

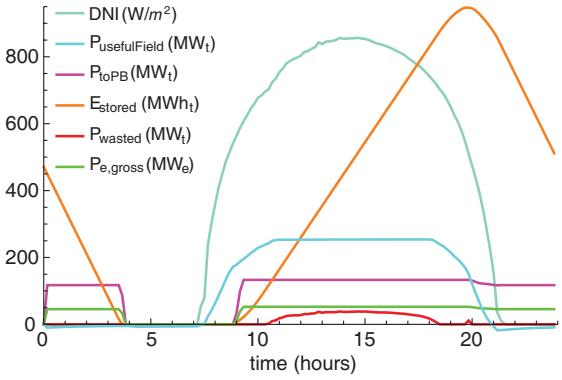

Figure 4: Example of simulation results for a summer day (July 6^{th}) for the plant considered in this paper.

power sent to the Power Block, stored energy, wasted solar power (see section 3.2.15) and gross electric power generated. Further details about results and calculations are given in the following sections.

The code is programmed in such a way that the main function calculates the operation of the plant for a single day. After a given day is calculated, certain results at the end of that day (HTF temperatures and energy stored in the TES system) are passed on as inputs for the calculation of the following day. The algorithm within the main function for a single day divides the calculations into several blocks: a night-time period before sunrise, a start-up period during which the HTF in the Solar Field is warmed up and the Power Block is started, a full-operation period during daylight hours, and a second night-time period after sunset. Within each of these blocks, the calculation proceeds point by point with the corresponding time step between consecutive data points (e.g. 1 hour, 10 minutes, etc.), and results are stored in lists so that, for a given data point, the algorithm can make use of the results from the previous time step. At the end of a simulation run, all variables used for the calculation of the electricity production of a plant can be exported to any spreadsheet or tabular text format, together with statistics on them (such as an average day for each month for an annual calculation, maximum and minimum values, etc.), as well as plotted as a function of time with the aim of allowing a detailed analysis of the results.

3.2. Detailed description of calculations

The following subsections explain the details of the relevant calculations within the model as outlined in the previous Fig. 3. Most of the time, these calculations have been particularised to the actual 50 MW_e plant simulated in this paper.

3.2.1. Geographical data

Geographical data for a given site location are required as input to the performance model. These include the latitude, φ, and longitude, λ, at the site, the longitude of the corresponding time-zone meridian, λ_{TZM}, the collector's orientation angle, γ_{col} (0 rad for North-South orientation and $\pi/2$ rad for East-West orientation) and the collector's tilt angle, β_{tilt} (angle of the collector's axis to the local horizontal, 0 rad for horizontal tracking axis).

3.2.2. Meteorological data

Meteorological data are usually provided in the form of a Typical Meteorological Year (TMY) representative of the chosen location. Our input format is based on the standard TMY3 format (Wilcox and Marion, 2008) and adjusted to any given time step between data points. Values of date and time, direct normal solar irradiance (E_b, in W/m^2), dry-bulb or ambient temperature (T_{amb}, in °C), wind speed (v_{wind}, in m/s), relative humidity (rh, in %) and atmospheric pressure (p_{amb}, in mbar) can be extracted from the TMY data. TMY data can be obtained, for instance, from the software *Meteonorm*, which makes use of databases from ground weather stations and satellite measurements to first obtain monthly values of meteorological data and then employs stochastic models to generate both daily and hourly values from those monthly values. Typical uncertainties are 10 – 20 % for solar irradiation and smaller than variations measured between one year and another.

While TMY data are typically used to simulate the expected electricity production of a plant, actual measurements of meteorological data at the location of an operating plant can also be used as input to the program in order to generate simulated results that can be compared to the actual production of a plant, as presented later in section 3.3.

The simulation code has been designed to function correctly for any time frequency of the input meteorological data (e.g., data given for every hour, every ten or fifteen minutes, etc.), since the time interval between consecutive data points is automatically detected in the first instances of the simulation.

3.2.3. Calculation of solar time

The procedure followed to calculate the solar time from the local time provided in the TMY data follows the steps in Stine and Geyer (2001). The solar time in hours, t_{solar}, for a given *day*, *month*, *year*, and local clock time (*hour* and *minute*), is given by the following expression:

$$t_{solar}(day, month, year, hour, minute) = \frac{minute}{60} + \\ + hour + \frac{(\lambda - \lambda_{TZM})}{15} + \frac{EOT(n_{leap})}{60} - \\ - DS(hour, day, month, year), \quad (1)$$

where λ is the longitude at the plant's site in degrees (positive if East of Greenwich Meridian, negative if West), λ_{TZM} is the longitude in degrees of the time zone meridian (there are 24 meridians, one per hour, separated by 15 degrees), EOT is the equation of time in minutes and DS is either 1 or 0 hours depending on whether the daylight savings time is in effect in the region or not.

Daylight savings can be taken into consideration by providing a list of specific daylight savings clock change times for a given location and for the years under study. By comparing the local time to the times in that list we can determine whether daylight savings applies or not. For instance, for Spain in the year 2000, clocks went forward one hour the 26th of March from 2*am* to 3*am* and back one hour the 29th of October at 3*am*. Therefore, for any time between these two, the value of $DS(hour, day, month, year)$ in Eq.(1) would be 1, and 0 for any other time that year.

The equation of time (Lamm, 1981) in minutes is calculated as follows:

$$EOT(n_{leap}) = 60 \sum_{i=0}^{i=5} A_{i+1}^{eot} \cos\left(\frac{\pi}{180} \frac{360 \cdot n_{leap}}{365.25} \cdot i\right) + \\ + 60 \sum_{i=0}^{i=5} B_{i+1}^{eot} \sin\left(\frac{\pi}{180} \frac{360 \cdot n_{leap}}{365.25} \cdot i\right), \quad (2)$$

where n_{leap} is the number of days into a leap-year cycle with 1 corresponding to January 1st of each leap year and 1461 to December 31st of the fourth year of the cycle (example leap years are 1960, 1964, 1968, ..., 2000, 2004, etc.). The corresponding lists of EOT coefficients are:

$$A^{eot} = 10^{-4} \times \{2.0870, 92.869, -522.58, -13.077, \\ -21.867, -1.5100\}, \\ B^{eot} = 10^{-4} \times \{0, -1222.9, -1569.8, -51.602, \\ -29.823, -2.3463\}, \quad (3)$$

with the suffix $i+1$ in Eq.(2) indicating position in these lists (from 1 to 6).

3.2.4. Calculation of the angle of incidence

The angle of incidence, θ, of the solar radiation on the parabolic trough collectors in the Solar Field is the angle between the direction of the incident radiation and

the normal to the collector's aperture. This angle determines the intensity of the radiation incident on the collector's mirror aperture area. Since the direct *normal* solar irradiance, E_b is by definition measured on a surface normal to its propagation direction, a factor $\cos(\theta)$ must be considered in order to calculate the total energy that can be focused and concentrated by the collectors onto the receiver tubes.

The angle of incidence is calculated following the explanations in Stine and Geyer (2001) for a single-axis tracking collector. The angle of incidence, θ, is calculated with Eq.(4) below, where γ_{col} and β_{tilt} (in radians) have been previously defined in section 3.2.1, and α_s and γ_s (in radians) are the solar altitude and solar azimuth angles respectively, which are in turn functions of the local date and time as given by the following expressions:

$$\alpha_s(day, month, year, hour, minute) = \sin^{-1}\left(\sin\delta \sin\left(\frac{\pi\varphi}{180}\right) + \cos\delta \cos\left(\frac{\pi\varphi}{180}\right)\cos\omega_{hour}\right), \quad (5)$$

$$\gamma_s(day, month, year, hour, minute) = \begin{cases} (2\pi - \gamma_s^0) & \text{if} \quad \omega_{hour} > 0\,, \\ \gamma_s^0 & \text{if} \quad \omega_{hour} \leq 0\,, \end{cases}$$
$$\gamma_s^0 = \cos^{-1}\left(\frac{\sin\delta\cos(\frac{\pi\varphi}{180}) - \cos\delta\sin(\frac{\pi\varphi}{180})\cos\omega_{hour}}{\cos\alpha_s}\right). \quad (6)$$

The previous expressions are functions of the site's latitude, φ, in degrees, the solar declination angle, δ, in radians and the hour angle, ω_{hour}, in radians, which are in turn functions of the local date and time as shown in the following equations:

$$\omega_{hour}(day, month, year, hour, minute) = \frac{15\pi}{180}\,(t_{solar}(day, month, year, hour, minute) - 12), \quad (7)$$

$$\delta(day, month, year) = \sin^{-1}\left(c_1 \cos\left[\frac{c_2\pi}{180}\,(n(day, month, year) - 173)\right]\right), \quad (8)$$

where $c_1 = 0.39795$, $c_2 = 0.98563$ and $n(day, month, year)$ is the number of days into the year (from 1 to 365 for a normal year and from 1 to 366 for a leap year).

3.2.5. Solar Field characteristics

Calculations in this paper simulate a 50 MW_e plant for which the Solar Field consists of 156 collector loops ($N_{loops} = 156$), a loop consists of 4 SCAs in series, forming two rows with two SCAs each, and a single SCA consists of 12 SCEs. The orientation of the collector's tracking axis is North-South. The parabolic trough collector (Castañeda et al., 2006; Fernández-García et al., 2010) specifications used throughout the calculations in this paper are the following: the gross[1] length and aperture width of a SCA are, respectively, $L_{sca,gross} = 150$ m and $w_{sca,gross} = 5.77$ m; the length of mirror in a SCA is $L_{sca} = 142.8$ m and the SCA mirror aperture area is $A_{sca} = 817.5\,m^2$; the gross loop aperture area and mirror aperture area are respectively $A_{c,gross} = 3462\,m^2$ and $A_c = 3270\,m^2$.

The optical efficiency is the fraction of incident solar energy that is absorbed by the receiver tubes in the Solar Field. The peak optical efficiency is defined as the optical efficiency at zero angle of incidence. It can be either measured experimentally on a fully assembled collector or estimated as follows:

$$\eta_{opt,0} = r\,\tau\,\alpha\; f_{apertLength}\; f_{assembly}\,, \quad (9)$$

where r is the reflectivity of the parabolic mirrors, τ is the transmissivity of the receiver's glass cover and α is the absorbance of the selective coating on the metallic pipe of the receiver tube, all of the former at normal incidence. Two factors which take values between 0 and 1 are included in the formula: $f_{apertLength}$ considers the reduction of effective absorbing receiver length due to shadowing of the bellows and HCE supports on the tube, and $f_{assembly}$ accounts for the reduction in energy absorbed by the receiver tube due to inaccuracies in the assembly of the collector components (structure, mirrors and HCE). The product of $f_{apertLength}$ and $f_{assembly}$ can also be referred to as intercept factor. Calculations for the plant considered in this paper use the following values: $r = 0.932$, $\tau = 0.96$, $\alpha = 0.95$, $f_{apertLength} = 0.954$ and $f_{assembly} = 1$, resulting in a peak optical efficiency $\eta_{opt,0} \simeq 0.81$.

The incidence angle modifier (k_{iam}) considers the effect of angles of incidence different from zero on the collectors optical efficiency. It is typically measured in experimental tests aimed to characterise a specific collector. Several expressions can be found in the literature for this factor. In this paper we use the expression from CIEMAT (2007), which gives k_{iam} as a fourth order polynomial in the angle of incidence, θ.

The row shadowing factor, $f_{rowShadow}$, accounts for the reduction of the effective mirror aperture area in the Solar Field due to shadows of collectors on one another,

[1] The term "gross" indicates that the length, width or aperture area of a SCA or collector, includes the small spaces between the individual mirror panels that form it.

$$\theta(day, month, year, hour, minute) = \cos^{-1}\left(\sqrt{1 - [\cos(\alpha_s - \beta_{tilt}) - \cos(\beta_{tilt})\cos(\alpha_s)(1 - \cos(\gamma_s - \gamma_{col}))]^2}\right), \quad (4)$$

particularly at times when the sun is low on the horizon. It takes values between 0 and 1 and it is the ratio of the effective collection width of an SCA over its gross width, as given by the following equation:

$$f_{rowShadow} = \max\left[0, \min\left[1, \frac{d_{row}}{w_{sca,gross}} \frac{\sin(\alpha_s)}{\cos(\theta)}\right]\right], \quad (10)$$

where d_{row} is the spacing between rows of collectors in the Solar Field, $w_{sca,gross}$ is the gross aperture width of the SCA, θ is the angle of incidence given by Eq.(4) and α_s is the solar altitude angle from Eq.(5).

The end loss factor, $f_{endLoss}$, accounts for the reduction of effective mirror aperture area caused by the spacing between SCAs and SCEs within a row of collectors in the Solar Field. It is calculated as the ratio of the effective length over the actual length of mirror in a SCA (L_{sca}), as deduced from geometrical considerations:

$$f_{endLoss} = 1 - \frac{m_2\, l_f \tan\theta}{L_{sca}} + \left(\frac{m_2 - 1}{L_{sca}}\right)\max[0, l_f \tan\theta - d_2] + \\ + \left(\frac{m_1 - 1}{m_1\, L_{sca}}\right)\max[0, l_f \tan\theta - d_1], \quad (11)$$

where m_1 is the number of SCAs in a row, m_2 is the number of SCEs within a SCA, d_1 is the spacing between consecutive SCAs in a row, d_2 is the spacing between consecutive SCEs in a SCA, l_f is the focal length of the parabola and θ is the angle of incidence. For the calculations in this paper we have used $d_{row} = 17.2\,\text{m}$, $l_f = 1.71\,\text{m}$, $m_1 = 2$, $m_2 = 12$, $d_1 = 1.5\,\text{m}$ and $d_2 = 0.25\,\text{m}$.

The Solar Field heat transfer fluid considered in this paper is *Therminol VP-1*, for which the density, specific heat and specific enthalpy are known functions of the fluid temperature. In this paper we have used 296°C and 390°C as design loop inlet and outlet HTF temperatures, respectively.

3.2.6. Power absorbed by a collector loop

The thermal power absorbed by the receiver tubes in a single collector loop is given by the following expression:

$$P_{absLoop} = E_b\, A_c\, \cos(\theta)\, \eta_{opt,0}\, k_{iam}(\theta) \times \\ \times f_{RowShadow}\, f_{endLoss}\, f_{clean}\, f_{dustEnv}\, \eta_{track}\, f_1, \quad (12)$$

where A_c is the mirror aperture area in a loop, f_{clean} is the mirror cleanliness factor (between 0 and 1), $f_{dustEnv}$ (between 0 and 1) considers the reduction in absorption due to dust on the receiver glass cover, η_{track} is the tracking error (between 0 and 1) and f_1 is an extra factor also between 0 and 1 to account for any additional reduction in energy absorption by the Solar Field loops. For the calculations in this paper we have used $f_{clean} = 0.97$, $f_{dustEnv} = 0.98$, $\eta_{track} = 0.99$ and $f_1 = 1$.

3.2.7. Receiver heat losses

Receiver thermal losses have a relevant impact in the final electricity production of a parabolic trough power plant and therefore need to be modelled as accurately as possible. Whereas it is possible to model these losses from first principles using a physical model, in this work we have chosen to use the empirical results obtained by NREL through heat-loss testing of several specific commercial receiver tubes.

For Solar Fields in which *Solel* receivers *UVAC2* and *UVAC3* are chosen, the empirical expressions for the measured heat loss reported in Burkholder and Kutscher (2008b) are used as follows:

$$HL_{uvac2}(T_{fl}, T_{amb}) = 0.43\,(T_{fl} + 5 - T_{amb}) + \\ + 1.09 \times 10^{-8}(T_{fl} + 5 - T_{amb})^4, \quad (13)$$

$$HL_{uvac3}(T_{fl}, T_{amb}) = 0.26\,(T_{fl} + 5 - T_{amb}) + \\ + 1.05 \cdot 10^{-8}(T_{fl} + 5 - T_{amb})^4, \quad (14)$$

where HL_{uvac2} and HL_{uvac3} are the heat losses in W/m (per unit length of receiver tube), T_{fl} is the average temperature in °C of the heat transfer fluid in the receiver tube, T_{amb} is the ambient temperature in °C, and it is assumed that the absorber temperature is always 5°C above the HTF temperature.

Alternatively, the empirical expression found in Burkholder and Kutscher (2008a) is used when *Schott*'s *2008 PTR70* receiver tubes are part of the Solar Field design. In this case, receiver heat losses are given as a function of the ambient temperature, wind speed, direct normal solar irradiance, angle of incidence and tube working condition. The average integrated heat loss in W/m is given by:

$$HL_{PTR70,i}(T_{in}, T_{out}, T_{amb}, E_b, v_{wind}, \theta) = \\ \frac{HL_{1,i} + HL_{2,i} + HL_{3,i} + HL_{4,i}}{(T_{out} - T_{in})}, \\ HL_{1,i} = (A_{0,i} + A_{5,i}\sqrt{v_{wind}})(T_{out} - T_{in}),$$

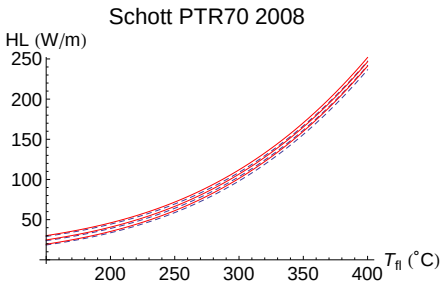

Figure 5: Heat loss in W per unit length of receiver tube as a function of average HTF temperature, T_{fl}, for evacuated Schott's 2008 PTR70 heat collection elements (Burkholder and Kutscher, 2008a). Solid red curves use an average HTF temperature assuming that there is a temperature jump of 100°C between input and output HTF temperatures ($T_{in} = T_{fl} - 50$°C and $T_{out} = T_{fl} + 50$°C), whereas dashed blue lines assume a constant HTF temperature throughout the receiver ($T_{in} = T_{fl} - 0.1$°C and $T_{out} = T_{fl}$). Both assumptions yield similar results. Lower curves correspond to an ambient temperature of 40°C, middle ones to 20°C and higher curves to 0°C. Receiver heat losses are shown to increase with increasing HTF temperature and decrease with increasing ambient temperature.

$$HL_{2,i} = (A_{1,i} + A_{6,i}\sqrt{v_{wind}})\left(\frac{T_{out}^2 - T_{in}^2}{2} - T_{amb}(T_{out} - T_{in})\right),$$
$$HL_{3,i} = \frac{A_{2,i} + A_{4,i}\cdot E_b \cdot \kappa_\theta \cdot \cos(\theta)}{3}(T_{out}^3 - T_{in}^3),$$
$$HL_{4,i} = \frac{A_{3,i}}{4}(T_{out}^4 - T_{in}^4), \qquad (15)$$

where T_{in} and T_{out} are the temperatures of HTF at the inlet and outlet of the receiver tube respectively, and the coefficients $A_{0,i}$ to $A_{6,i}$ vary depending on whether the receiver tubes are evacuated, have lost vacuum, have hydrogen in the inter-annular space or are broken (possibilities indicated by the suffix $_i$), as given by Table 8 in Burkholder and Kutscher (2008a). The final heat loss is given by Eq.(16) as follows:

$$HL_{PTR70}(T_{in}, T_{out}, T_{amb}, E_b, v_{wind}, \theta) = \sum_i F_i \cdot HL_{PTR70,i}, \qquad (16)$$

where F_i indicate the corresponding fractions of receiver tubes in good and deteriorated conditions in the Solar Field. This heat loss can also be given as a function of the average temperature of the HTF in the receiver tubes, T_{fl}, as evidenced by Fig. 5, which shows the dependence of *PTR70* receiver thermal losses on average HTF temperature for a range of ambient temperature conditions.

3.2.8. Piping thermal losses

Solar Field piping heat losses are calculated making use of an empirical equation (Patnode, 2006) derived per unit Solar Field aperture area for the SEGS plants in the USA. The thermal loss in Watts as a function of the difference between ambient temperature and average HTF temperature is calculated as:

$$P_{pipeLoss} = N_{loops}A_{c,gross}(0.01693\Delta T - -1.683\times10^{-4}\Delta T^2 + 6.78010^{-7}\Delta T^3),$$
$$\Delta T = T_{fl,pipes} - T_{amb}, \qquad (17)$$

where N_{loops} is the number of collector loops in the Solar Field, $A_{c,gross}$ is the gross loop aperture area and $T_{fl,pipes}$ is the average HTF temperature in the insulated pipes.

3.2.9. Calculation of HTF temperatures

HTF temperatures (see Fig. 3) at a given instant determine the decision to operate the plant in one configuration or another, as detailed in the following section 3.2.15.

If we consider a pipe portion that can contain a mass of fluid m at a temperature T, and which receives an input mass flow rate $\dot{m}$ at temperature T_{in}, while losing an output mass flow rate also equal to $\dot{m}$ at temperature T, and which exchanges heat with its surroundings at a rate $\dot{Q}_{ext}$ (positive for heat gain from solar irradiation and negative for heat losses), we can write the heat-balance equation for the system as:

$$\frac{dH}{dt} = mc_p\frac{dT}{dt} = \dot{m}c_pT_{in} - \dot{m}c_pT + \dot{Q}_{ext}, \qquad (18)$$

where H is the enthalpy of the thermodynamic system, t is time and c_p is the fluid's specific heat at constant pressure, which is a function of the fluid's temperature. We have assumed that $dH \approx dQ$, where Q is heat, hence neglecting any pressure changes for the liquid HTF within a given pipe portion. From this, we have that:

$$\frac{dT(t)}{dt} = \frac{\dot{m}\,(T_{in}(t) - T(t))}{\rho(T(t))V} + \frac{\dot{Q}_{ext}}{\rho(T(t))Vc_p(T(t))}, \qquad (19)$$

where the mass, m, of fluid inside the pipe portion at a given instant has been substituted for $\rho(T(t))V$, where ρ is the density of the fluid, which in turn depends on the fluid's temperature, and V is the inner volume of the pipe portion. The second term in Eq.(19) corresponds to the temperature change that the fluid would experience being at rest, while the first term has opposite sign to the second and accounts for the fact that the fluid is circulated through the pipe at a flow rate $\dot{m}$, reducing the overall rate of its temperature change.

The simplest model considered for the Solar Field is a closed circuit in which all collector loops are considered equivalent, each with four different portions of uninsulated pipe (one portion around 150 m-long for each

SCA), and with another large pipe portion for the Solar-Field insulated pipes. This pipe circuit model would apply during the initial stage of the HTF warm-up period, when the fluid circulates through the Solar Field bypassing the Power Block heat exchangers. In this case, we can perform a full calculation of the HTF temperatures in the Solar Field by solving a system of five coupled differential equations (one per pipe portion in the model), each of the same form as Eq.(19), providing initial conditions for the temperatures in each of the five pipe portions at $t = 0$. Doing this yields time-dependent expressions for the HTF temperatures in the Solar Field: $T_1(t)$, $T_2(t)$, $T_3(t)$, $T_4(t)$ and $T_{pipes}(t)$, where T_1 to T_4 refer to the average HTF temperatures within each SCA in a loop going from inlet to outlet, and T_{pipes} refers to that in the insulated pipes. Even if solving similar systems of coupled differential equations during the full calculation of a solar thermal plant annual production is possible, it is not practical in terms of calculation time, and it is therefore convenient to avoid this approach. However, the full detailed solution can be used as reference in order to make sure that any approximation taken is a valid one.

We can simplify the problem by assuming a linear and discrete approximation for Eq.(19) where we have $dT(t)/dt \approx \Delta T/\Delta t = (T - T_0)/\Delta t$, where T_0 and T indicate the HTF temperatures in a given pipe portion at the beginning and end of a time interval Δt, respectively. Hence, solving for T, we have:

$$T = \frac{T_0 + \left(\frac{\dot{m}}{\rho(T(t))V} T_{in} + \frac{\dot{Q}_{ext}}{\rho(T(t))Vc_p(T(t))}\right)\Delta t}{\left(1 + \frac{\dot{m}}{\rho(T(t))V}\Delta t\right)}, \qquad (20)$$

where we have assumed that the variation of ρ and c_p with temperature is slow and hence negligible over a short enough time interval Δt. Therefore, the solution for the HTF temperatures at the end of a time interval Δt is given by the following set of equations:

$$T_1 = \frac{T_{1,0} + \left(\frac{\dot{m}_{loop}}{\rho(T_{1,0})V_{SCA}} T_{pipes,0} + \frac{P_{usefulLoop}}{\rho(T_{1,0})V_{SCA}c_p(T_{1,0})}\right)\Delta t}{\left(1 + \frac{\dot{m}_{loop}}{\rho(T_{1,0})V_{SCA}}\Delta t\right)},$$

$$T_2 = \frac{T_{2,0} + \left(\frac{\dot{m}_{loop}}{\rho(T_{2,0})V_{SCA}} T_{1,0} + \frac{P_{usefulLoop}}{\rho(T_{2,0})V_{SCA}c_p(T_{2,0})}\right)\Delta t}{\left(1 + \frac{\dot{m}_{loop}}{\rho(T_{2,0})V_{SCA}}\Delta t\right)},$$

$$T_3 = \frac{T_{3,0} + \left(\frac{\dot{m}_{loop}}{\rho(T_{3,0})V_{SCA}} T_{2,0} + \frac{P_{usefulLoop}}{\rho(T_{3,0})V_{SCA}c_p(T_{3,0})}\right)\Delta t}{\left(1 + \frac{\dot{m}_{loop}}{\rho(T_{3,0})V_{SCA}}\Delta t\right)},$$

$$T_4 = \frac{T_{4,0} + \left(\frac{\dot{m}_{loop}}{\rho(T_{4,0})V_{SCA}} T_{3,0} + \frac{P_{usefulLoop}}{\rho(T_{4,0})V_{SCA}c_p(T_{4,0})}\right)\Delta t}{\left(1 + \frac{\dot{m}_{loop}}{\rho(T_{4,0})V_{SCA}}\Delta t\right)},$$

$$T_{pipes} = \frac{T_{pipes,0}}{\left(1 + \frac{N_{loops}\dot{m}_{loop}}{\rho(T_{pipes,0})V_{pipes}}\Delta t\right)} + \frac{\left(\frac{N_{loops}\dot{m}_{loop}}{\rho(T_{pipes,0})V_{pipes}} T_{4,0} + \frac{-\dot{Q}_{pipeLoss}}{\rho(T_{pipes,0})V_{pipes}c_p(T_{pipes,0})}\right)\Delta t}{\left(1 + \frac{N_{loops}\dot{m}_{loop}}{\rho(T_{pipes,0})V_{pipes}}\Delta t\right)}, \qquad (21)$$

where the temperatures at the beginning of the time interval are considered to be known values: $T_{1,0}$, $T_{2,0}$, $T_{3,0}$, $T_{4,0}$ and $T_{pipes,0}$, the mass flow rate within a collector loop is $\dot{m}_{loop}$, N_{loops} is the number of loops in the Solar Field, $P_{usefulLoop}$ is the useful thermal power collected by a loop after subtracting receiver heat losses, and $\dot{Q}_{pipeLoss}$ is the piping heat loss. For the calculations in this paper, we have assumed that the volume of HTF within the receiver tubes in a SCA, V_{SCA}, is approximately $0.5\,\mathrm{m}^3$, while that in the insulated pipes, V_{pipes}, is considered to be approximately $1400\,\mathrm{m}^3$.

In order to find the evolution of the HTF temperatures during a given time interval, t_{data} (1 hour or 10 minutes, for instance), we can break the problem into a number of smaller time steps Δt and iteratively obtain the fluid temperatures making use of Eqs.(21). For this linear and discrete approximation to be valid, the time step of the calculation must be small enough, $\Delta t \leq 10\,\mathrm{s}$, for the results to agree within $1 - 2\,^\circ\mathrm{C}$ with the solution of the full system of differential equations. Calculation steps longer than 10 seconds lead to larger errors in the calculation of HTF temperatures.

Several simplified models can be constructed in a similar fashion. The simulation makes use of three different predefined functions which follow this methodology to find solutions for the HTF temperatures iteratively, using a calculation step of 10 seconds. The first function is the one described above (4 SCA portions and 1 portion for insulated pipes, with the HTF bypassing the Power-Block heat exchangers), the second function includes the Power-Block heat exchangers in the HTF circuit by fixing the temperature of the incoming flow to the first SCA to the value of the design loop inlet temperature, and the third function accounts for the freeze-protection system for HTF (see section 3.2.11) by considering the four SCAs in each loop, two different portions of insulated pipes, and the HTF-heater portion in between them, which receives a heat input according to the heater specifications.

Despite the fact that these simplified models consider only one or two large insulated pipe portions within the Solar Field HTF circuit, calculations derived from them are in very good agreement with actual measurements in an operating plant, as demonstrated in the later section 3.3. This owes to the fact that the models calculate

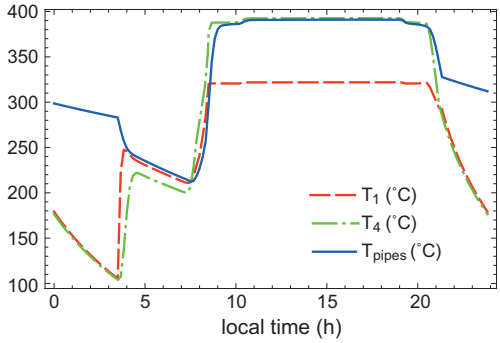

Figure 6: Example of the HTF temperatures calculated during 24 hours. **Solid blue line**: calculated average HTF temperature in the insulated pipes, T_{pipes} (Solar Field output). **Dashed red line**: calculated average HTF temperature in the first SCA of a loop, T_1. **Dot-dashed green line**: calculated average HTF temperature in the fourth SCA of a loop, T_4 (loop outlet). The corresponding simulated HTF mass flow rates per loop and operating conditions are those shown in Fig. 10 for July 13th 2010.

average HTF temperatures representative of each pipe portion by properly taking into account the volume of HTF within each portion.

Fig. 6 shows an example of the results for the HTF temperatures T_1, T_4 and T_{pipes} calculated during a full day. The corresponding HTF mass flow rate through each loop is that shown in the first 24 hours in Fig. 10. In this example, the HTF does not circulate in the Solar Field until around 4 *am*, and cools down accordingly. Since the receiver tubes are not insulated, the temperatures at the loop inlets and outlets, T_1 and T_4, respectively, fall much faster than the HTF temperature in the insulated pipes. At around 4 *am*, the HTF starts to circulate through the Solar Field (using the circulation pumps and bypassing the Power Block) at a rate of 1 kg/s per loop. As a consequence, the temperature in the loops increases while that in the insulated pipes decreases, given the larger volume of hotter HTF in the insulated pipes. When the sun rises at around 7-8 *am*, the mass flow rate increases to 2.5 kg/s per loop and the HTF warms up thanks to the solar radiation until the design operating conditions are reached (see section 3.2.15) and an equilibrium is maintained. At around 20-21 *pm*, with sunset, the HTF circulation through the Solar Field stops and both the HTF in the collector loops and in the insulated pipes cool down at their corresponding rates.

3.2.10. Solar Field useful thermal power

The thermal power absorbed by a collector loop, $P_{absLoop}$, is calculated as given by Eq.(12) and then limited to a maximum value, $P_{absLoop,max}$, which is calculated as the product of the maximum HTF mass flow rate in a loop (see section 3.2.14) and the HTF specific enthalpy increase from the design inlet to outlet temperatures, with an additional factor of ~ 1.1 to account for receiver thermal losses. In this paper we have used $P_{absLoop,max} \simeq 1.8\,\mathrm{MW_t}$. This limit guarantees that the HTF temperature at the loop outlets does not surpass its maximum design value. In an actual plant, control of the HTF loop-outlet temperatures under high solar radiation conditions is realised through the deliberate de-focusing of a number of collectors within a loop, in order to avoid damage to the HTF. The fraction of collectors that remain in focus is calculated as the ratio of the thermal power absorbed by a loop after the limitation is applied to the same power before the limit is applied.

HCE thermal losses are obtained using the average HTF temperatures in each SCA at the end of the previous time step (see section 3.2.9). For the results shown in this paper, the total HCE losses in a loop are calculated as: $\sum_{k=1}^{k=4} HL_{uvac3,k}(T_{fl,k}, T_{amb}) \times l_{hce,sca}$, where k indicates the corresponding SCA in the loop and $l_{hce,sca} = 146.16\,\mathrm{m}$ is the total length of receiver tubes in a SCA (36 HCEs per SCA, each 4.06 m-long). The total HCE losses in a loop are subtracted from the thermal power absorbed by a loop, and the result is then multiplied by the number of loops in the Solar Field. Solar Field piping losses are obtained from Eq.(17) using the average HTF temperature in the insulated pipes calculated for the end of the previous time step (see section 3.2.9), and subtracted from the previous result to obtain the useful thermal power collected by the Solar Field.

3.2.11. HTF freeze-protection system

A freeze-protection system for the HTF in the Solar Field is implemented by considering the thermal power provided by the HTF heaters. This system is triggered when the HTF loop outlet temperatures fall below a given value, $T_{antifreeze-on}$, and functions until it reaches a second higher value, $T_{antifreeze-off}$. For the calculations in this paper, we have assumed that the HTF heaters provide a thermal power of $10\,\mathrm{MW_t}$ in antifreeze mode, $T_{antifreeze-on} = 60°\mathrm{C}$, $T_{antifreeze-off} = 100°\mathrm{C}$, the volume of HTF that is heated up inside the HTF heaters is $10\,\mathrm{m^3}$ and the HTF mass flow rate circulated by the freeze-protection pumps is 1 kg/s per collector loop in the Solar Field.

3.2.12. Power Block model

A certain amount of thermal power is delivered to the Power Block from the Solar Field or the TES system (or both), for the production of electricity in the turbine and

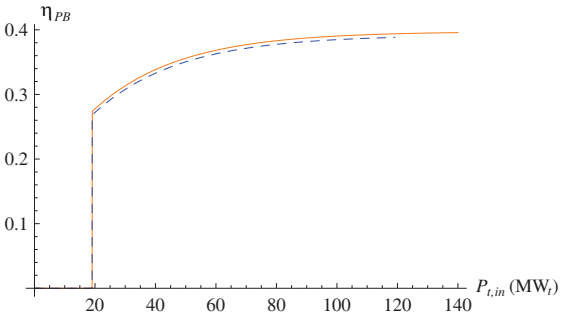

Figure 7: Power Block efficiency for conversion of input thermal power into electric power in solar-only mode (solid orange line) and storage mode (blue dashed line) as a function of input thermal power.

generator. The efficiency of the corresponding heat exchangers (HTF to water-steam) determines the thermal power input to the Power Block on the water-steam side and is considered to be $\eta_{exch} = 0.95$.

The efficiency of the power cycle in terms of the fraction of thermal input which is converted to electricity, depends on the thermal input power as well as on the ambient conditions. However, for the results presented in this paper, only the dependence on the former has been considered. The efficiency of the Power Block, η_{PB}, in **solar-only mode** (generating electricity directly from the heat delivered by the Solar Field) is calculated as $\eta_{PB}(P_{t,in}) = a_1 + a_2 \exp(-P_{t,in}/a_3)$, where $P_{t,in}$ is the thermal power input to the Power Block (water-steam side) in $\mathrm{MW_t}$, and the coefficients used for the $50\,\mathrm{MW_e}$ plant simulated in this paper are $a_1 = 0.397$, $a_2 = -0.243$ and $a_3 = 28.23\,\mathrm{MW_t}$, obtained from a fit of the turbine's specification data provided by a supplier.

The efficiency operating in **storage mode** (generating electricity exclusively from the heat delivered by the TES system) is lower and assumed to be a similar curve to the previous one but displaced from it by $\sim -0.6\%$ (inferred from supplier data for storage mode). The minimum thermal input that results in an electricity production different from zero (technical minimum) is chosen to be $\sim 19\,\mathrm{MW_t}$ for both operating modes, as shown in Fig. 7.

When the plant operates in a mixed mode in such a way that thermal power is sent to the Power Block from both the Solar Field and the TES system, the turbine efficiency is calculated as the weighted average of the efficiencies for solar-only and storage modes, using the fractional HTF mass flow rates sent to the Power Block from the Solar Field and from the TES system, respectively, as weights.

The actual gross electric power, $P_{e,gross}$, generated from a given thermal power, $P_{t,in,htf}$ on the HTF side ($\eta_{exch}\,P_{t,in,htf}$ on the steam side), sent to the Power Block, is therefore given by $P_{e,gross} = \eta_{exch}\,P_{t,in,htf} \times \eta_{PB}(\eta_{exch}\,P_{t,in,htf})$ in solar-only mode, and similarly with the corresponding efficiencies, for the storage and mixed operating modes.

An update of this simplified model is currently under development to include the influence of both ambient temperature and relative humidity on the electricity output from the Power Block.

3.2.13. Thermal Energy Storage (TES) system

In this paper we assume that the TES system is a two-tank molten-salt system (our simulation can include up to three pairs of molten-salt tanks). The salts are a mixture of Sodium and Potassium Nitrates with known properties of density and specific heat as a function of temperature.

During a typical storage charge, the excess thermal power delivered by the Solar Field is sent to the TES circuit, so that part of the HTF passes through the HTF-TES heat exchangers in order to transfer and store heat in the TES fluid. During storage discharge, the opposite process takes place and heat is transferred from the TES fluid to the HTF and then typically delivered to the Power Block. The efficiency of the HTF-TES heat exchangers is assumed to be $\eta_{exch-TES} = 0.95$. The maximum amount of energy stored as heat in the TES system is given by its total storage capacity, which is assumed to be $1010\,\mathrm{MWh_t}$ for the calculations in this paper and corresponds to approximately 7.5 equivalent hours of operation at the Power Block's design input level.

The model for the TES system performs all calculations in terms of thermal power delivered to or extracted from it. The algorithm considers in detail the available thermal powers, the state of the storage tanks and all the equipment limitations (see section 3.2.14) to decide how much thermal power can be sent to storage or extracted from it. The known salt properties at the design temperatures in the hot and cold salt tanks (assumed to be 386°C and 292°C, respectively) are used to calculate the corresponding molten salt mass flow rate between the tanks during storage charge or discharge. This mass flow rate is in turned used to calculate the parasitic electricity consumption of the salt pumps. On the HTF side, the design HTF temperatures during storage charge are considered to be 298°C and 393°C on the cold and hot ends, respectively, and 360°C and 290.5°C, during storage discharge.

3.2.14. Parameter limitations

The HTF mass flow rate through a collector loop in the Solar Field is assumed to be limited to a minimum of $\sim 2\,\mathrm{kg/s}$ per loop to guarantee a turbulent HTF flow with a Reynolds number of at least 2×10^5, for an efficient heat transfer between the heat collected in the receiver tubes and the HTF flowing through them. This limit applies in the simulation when the HTF in the Solar Field is circulated by the main HTF pumps (see Fig. 2) and when the collectors are tracking the sun and the HTF in the Solar Field has gone through an initial warm-up period (see section 3.2.15).

A maximum limit of $1100\,\mathrm{kg/s}$ for the HTF mass flow rate in the Solar Field as a whole is also enforced, as given by the specifications of the main HTF pumps. This limit corresponds to a maximum of $\sim 7\,\mathrm{kg/s}$ of HTF per loop. This in turn leads to the limitation for the thermal power absorbed by a collector loop, $P_{absLoop,max} \simeq 1.8\,\mathrm{MW_t}$, as mentioned in section 3.2.10. Any incident solar power in excess of this is therefore wasted.

The maximum thermal power (HTF side) which can be sent to the Power Block from the Solar Field during solar-only operation is considered to be $P_{maxCS\,toPB} \simeq 140\,\mathrm{MW_t}$, which leads to a maximum gross electric power generated of $\sim 52.6\,\mathrm{MW_e}$, at a maximum Power Block efficiency (η_{PB}) of 39.5%.

Certain limits are considered during TES charge and discharge due to molten salt pumps and heat-exchanger limitations. A minimum HTF mass flow rate of $90\,\mathrm{kg/s}$ is assumed for both storage charge and discharge. This leads to a minimum allowable HTF thermal power of $\sim 21\,\mathrm{MW_t}$ sent to the TES system during storage charge, calculated using the previous minimum HTF flow rate and the HTF temperatures during storage charge under design conditions (see section 3.2.13). Similarly, the minimum thermal power during storage discharge is taken to be $\sim 15\,\mathrm{MW_t}$ on the HTF side, or $\sim 16\,\mathrm{MW_t}$ on the salt side when considering $\eta_{exch-TES}$. Due to heat-exchanger limitations and in order to match the actual plant data, the maximum thermal power on the HTF side during TES charge is limited to $\sim 100\,\mathrm{MW_t}$, whereas during TES discharge it is limited to $\sim 124\,\mathrm{MW_t}$. On top of that, there is a maximum limit of $\sim 113\,\mathrm{MW_t}$ for the thermal input to the turbine on the steam side as specified by the turbine balance for storage mode operation. This imposes an effective limit of $P_{maxTES\,toPB} \simeq 119\,\mathrm{MW_t}$ on the thermal power on the HTF side during storage discharge. Both limitations are included to account for the fact that the heat-exchanger limitation could be more stringent than the turbine-input one.

When the plant operates neither in solar-only mode nor in storage-only mode, but in a mixed mode in which energy is sent to the Power Block from both the Solar Field and the TES system, the limitation that applies to the thermal input sent to the turbine is a value between $P_{maxTES\,toPB}$ and $P_{maxCS\,toPB}$, calculated as $P_{toPB\,fromCS} + (1 - P_{toPB\,fromCS}/P_{maxCS\,toPB})P_{maxTES\,toPB}$, where $P_{toPB\,fromCS}$ is the thermal power sent to the Power Block from the Solar Field, which in this mixed mode is larger than zero and lower than $P_{maxCS\,toPB}$.

Note that the simulation can include up to three pairs of molten-salt storage tanks. In this case, two or three inter-dependent TES systems are considered, with the TES limitations explained above applying to each pair of tanks, and the state of each TES system being accounted for during TES charge and discharge. The TES systems with more energy stored are favored during storage discharge, while those with less accumulated energy are favored during storage charge.

3.2.15. Simulated plant's operation strategy

As outlined in section 3.1, the algorithm that calculates a single day is divided into several blocks: a night-time period before sunrise, a period for warm-up of the HTF in the Solar Field and start-up of the Power Block, a full-operation period during daylight hours and a second night-time period after sunset.

The decisions implemented in the algorithm are those that best reproduce the actual operating decisions taken in the plant under study in this paper, on the corresponding dates shown in section 3.3.

During any of the **night-time periods**, the algorithm first checks if TES discharge is possible taking into account the state of the TES system and the limitations explained in section 3.2.14. If storage discharge is possible, the plant generates electricity operating in storage mode and the HTF does not circulate in the Solar Field (this choice is made to match the actual plant data which correspond to summer days). Storage discharge continues during night hours until no useful energy remains stored in the TES system.

If storage discharge is not possible, no electricity is generated by the turbine. The HTF remains still in the Solar Field unless the calculated loop-outlet temperature (T_4 in section 3.2.9) falls below a certain input value, $T_{HTFcircul}$, in which case, the HTF is circulated through the Solar Field at $1\,\mathrm{kg/s}$ (input value) per loop by means of the HTF circulation pumps (see Fig. 2). For the results presented in this paper and in order to match the actual plant data, $T_{HTFcircul} = 400^\circ\mathrm{C}$, meaning that the HTF is effectively always circulated if no TES discharge is taking place.

If the HTF temperature at the loop outlets falls further, below 60°C (input value), the freeze-protection system for HTF is activated, as explained in section 3.2.11.

The **HTF warm-up and turbine start-up periods** begin with sunrise and last until the HTF reaches its design Solar Field outlet temperature and the turbine reaches 100% steam input load. During the **HTF warm-up period**, the useful thermal power collected by the HCEs in the Solar Field heats up the HTF in the loops and the electric power output of the plant is zero. The slow temperature rise of the HTF in the Solar Field is calculated as detailed in section 3.2.9. In a first stage, the HTF circulates through the loops at a mass flow rate $\dot{m}_{heatHTF}$ (chosen to be 2.5 kg/s per loop) and bypassing the Power-Block heat exchangers until the calculated HTF temperature in the first SCA of each loop (T_1) reaches the design inlet value (296°C). After that, in a second stage, the HTF goes through the Power-Block heat exchangers until the temperature of the HTF in the insulated pipes (T_{pipes}) reaches a value lower than the design loop outlet temperature (390°C) by a given margin ΔT_{margin} (80°C for the results shown). In this second stage, the HTF circulates at the maximum between the calculated HTF mass flow rate $\dot{m}_{calc}$ (see text below) and the minimum loop flow rate (see section 3.2.14).

After the HTF warm-up period, the **start-up of the turbine** is modelled by means of an additional 20-minute-long period (hot start) over which the turbine's input load increases linearly from 0% to 100%, and electricity begins to be generated.

These assumptions are made after consideration of the start-up curves for a 50 MW_e turbine and of operating plant data. The agreement of the HTF heat rates and turbine start-up calculated in this way with actual data from an operating 50 MW_e plant is very good, confirming the validity of this method. Note that, since the calculated HTF temperature increase in the insulated pipes is relatively slow, the actual heat-exchanger limitation during HTF warm-up of $\sim$ 4°C/minute, as stated by equipment suppliers, is typically not surpassed.

The **full-operation period** during daylight hours follows the HTF warm-up and turbine start-up periods and continues until sunset. As explained before, the plant starts generating electricity after the HTF temperature in the Solar Field insulated pipes reaches a value above the design loop outlet temperature minus ΔT_{margin}.

A maximum wind speed for the operation of the collectors on sun-tracking mode is implemented in the model by assuming that no thermal power is absorbed at times when the actual wind speed exceeds such maximum ($\sim$ 14 m/s), since collectors would be facing the ground (stow mode) for safety on these occasions.

Fig. 8 shows a schematic diagram of the algorithm decisions during the full-operation period. If due to low solar radiation the turbine stopped generating electricity in the previous time step, two cases are considered: if the solar radiation is still low and $P_{absLoop}$ (see section 3.2.6) is not above 20 kW_t, the algorithm proceeds as in the night-time periods with no storage discharge and the HTF in the Solar Field cools down; if the solar radiation is high enough for $P_{absLoop}$ to be above 20 kW_t, the algorithm proceeds as in the HTF warm-up period. The value of 20 kW_t is used to discriminate between HTF warming up or cooling down and it corresponds to the approximate HCE thermal losses in a loop at design conditions. The condition $P_{absLoop} > 20\,kW_t$ therefore points to the useful thermal power in a loop being greater than zero.

Hence, if at some point during daylight hours, a cloudy period has made the turbine stop, the HTF will need to be warmed up again and the plant will need to go through a second start-up process. Depending on meteorological conditions, several start-ups can occur within a single day.

On the other hand, if the turbine was generating electricity in the previous time step and the HTF temperature in the insulated pipes has stayed above the design loop outlet temperature minus ΔT_{margin}, the following steps are taken, as shown in Fig. 8. The calculated HTF mass flow rate in a loop, $\dot{m}_{calc}$, is obtained from the HTF specific enthalpy change within a single loop at design inlet and outlet temperatures and from a preliminary estimation of the useful thermal power in a loop. This estimation assumes an average of the design inlet and outlet HTF temperatures to calculate a first estimate of the HCE losses. The resulting HTF mass flow rate is then limited to its maximum allowable value as indicated in section 3.2.14, and to values ≥ 0. Once an operating HTF mass flow rate through the Solar Field has been chosen according to the diagram in Fig. 8, the HTF temperatures (in each SCA and in the Solar Field insulated pipes) can be calculated as detailed in section 3.2.9. The HTF temperatures at the end of the previous time step are used to obtain the final HCE and piping thermal losses, which lead to a final value for the useful thermal power captured by the Solar Field. This value determines the operation of the plant as shown in the figure. If the solar radiation is low and the calculated $\dot{m}_{calc}$ is below the minimum HTF mass flow rate in a loop during solar operation ($\sim$ 2 kg/s), the algorithm decides to keep the HTF flow rate at that minimum value. In

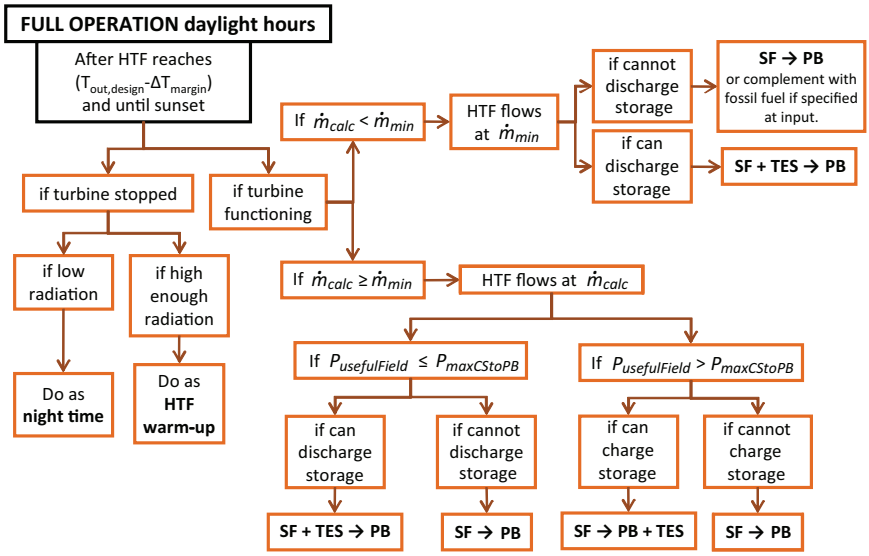

Figure 8: Schematic for the decisions taken by the algorithm during the full-operation period on daylight hours. SF stands for Solar Field, PB, for Power Block, TES, for thermal energy storage system, $\dot{m}_{calc}$ is the calculated HTF mass flow rate in a loop (see text), $\dot{m}_{min}$ is the minimum HTF mass flow rate in a loop, $P_{usefulField}$ is the useful thermal power captured by the Solar Field after all losses have been subtracted (see section 3.2.10) and $P_{maxCStoPB}$ is the maximum thermal input to the Power Block on the HTF side during solar-only operation.

this case, the plant operates by sending all the useful power collected in the Solar Field to the Power Block and complementing it with additional power from the TES system if storage discharge is possible.

The power sent to the turbine from the Solar Field on the HTF side is calculated from the product of the chosen HTF mass flow rate and the HTF specific enthalpy change when going from the calculated Solar Field outlet temperature to the design Solar Field inlet temperature (the calculated T_{pipes} is considered as the HTF temperature into the Power Block and 296°C is considered as a fixed Power Block HTF outlet temperature). Under low radiation conditions, the HTF which flows in the Solar Field and then reaches the Power Block takes some time to cool down, allowing the delivery of non-zero thermal power to the turbine for some time, even if the instantaneous useful thermal power in a loop is low.

The power sent to the turbine from the TES system is calculated considering the amount of energy stored in the TES system, the remaining thermal power that can be sent to the turbine to complete its maximum thermal input after accounting for the power sent to it from the Solar Field, and the power limitations during storage discharge in storage-only or mixed mode as stated in section 3.2.14.

Continuing with the diagram in Fig. 8, when the solar radiation is high enough for the calculated HTF mass flow rate, $\dot{m}_{calc}$, to be above the minimum one, $\dot{m}_{calc}$ is used as the operating flow rate. The power sent to the turbine from the Solar Field is calculated the same way as in the case of low radiation and it is the value of the useful thermal power collected by the Solar Field that determines the plant's operating mode. If this power is below or equal to the maximum thermal power (HTF side) that can be sent to the Power Block from the Solar Field, $P_{maxCStoPB}$, the operation is similar to that explained for low radiation conditions except for the different chosen HTF mass flow rate. If, on the other hand, the Solar Field useful thermal power exceeds $P_{maxCStoPB}$, the power sent to the Power Block from the Solar Field (on the HTF side) is precisely $P_{maxCStoPB}$, and any power in excess of that is sent to the TES system if it is possible after consideration of the state of the storage system and the corresponding limitations for storage charge (see section 3.2.14), or wasted if not.

Thermal power can be wasted due to the fact that the mass flow rate in a collector loop has a maximum limitation, due to the limits of maximum and minimum thermal powers that can be sent to the turbine and to the TES system during storage charge, and due to the fact that at times, the TES system might be at its maximum storage capacity so that no more energy can be stored.

The simulation provides the user with the option to

use or not fossil fuel for charging the TES system at night, or to complement the thermal input to the Power Block during the day, when the radiation is low, on specific dates of choice. However, this has not been considered for the results presented in section 3.3.

3.2.16. Parasitics

A detailed calculation of parasitic electric consumption can be carried out based on the characteristics of the specific equipment for a given plant. Offline parasitics are those taking place when the gross electric power generated is zero, as opposed to online parasitics. Solar Field parasitics include main HTF pumps, HTF circulation pumps, tracking and communication system for the Solar Field, HTF system (lubrication, expansion, ullage, HTF heaters, electrical heating). Power Block parasitics include condensate pumps, feedwater pumps, water circulation pumps, closed/open loop refrigeration pumps, service water pumps, cooling tower, balance of plant consumption, water treatment plant, auxiliary heaters, compressed air system and electrical losses.

Simulated results for parasitic consumption are not presented in this paper, since the corresponding actual data was not available for comparison.

3.3. Simulation results and comparison to actual plant data

Actual data from the plant *Andasol 2*, operated by the ACS Industrial Group in Granada, Spain, was kindly made available to Initec-Energía. These data correspond to 42 summer days, from June 26$^{\text{th}}$ to August 6$^{\text{th}}$ of 2010, with the time step between data points being ten minutes.

The simulation described in the previous sections was run using as input the actual data measured at the site's weather stations for E_b, T_{amb}, v_{wind} and rh. Where data from more than one station were available, an average value was calculated. The actual data used for comparison with the simulation results are described as follows.

The actual thermal energy accumulated in the TES system is calculated from the measured temperature, $T_{hotSalt}$, and level, $l_{hotSalt}$, of the hot salts in the hot storage tank, as given by the following equations:

$$E_{stored}(\mathrm{MWh_t}) = \frac{10^{-6}}{3600}\, m_{hotSalt} \times c_{p,salt}(T_{hotSalt}) \times \\ \times (T_{hotSalt} - T_{coldSalt,design})\,,$$

$$m_{hotSalt} = \rho_{salt}(T_{hotSalt})\,\pi \left(\frac{D_{tank}}{2}\right)^2 (l_{hotSalt} - l_{min}),$$

where $m_{hotSalt}$ is the mass in kg of molten salts stored in the hot salt tank, $c_{p,salt}(\mathrm{J/(kgK)}) = 1443 + 0172\, T_{hotSalt}$, with the temperature in °C, is the assumed molten salt specific heat, $\rho_{salt}(\mathrm{kg/m^3}) = 2090 - 0.636\, T_{hotSalt}$ is the temperature-dependent molten salt density, the design temperature of the salts in the cold tank is assumed to be $T_{coldSalt,design} = 292$°C, the diameter of the tank's base is taken to be $D_{tank} = 38.5$ m and a value $l_{min} = 0.6$ m is assumed to be the minimum level that the salts need to reach in the tank for the salt pumps to be able to extract any salts from it.

Actual data for the temperature of the HTF into the Power Block, just after the HTF flows out of the Solar Field and TES system are combined, is also available and can at times be compared to the simulated HTF temperature at the output of the Solar Field (calculated T_{pipes}). Actual data for the HTF temperature at the Solar Field outlet was not available. Note that the actual and simulated HTF temperatures refer to different points in the HTF circuit and can only agree at the times when no TES discharge takes place. During TES discharge, the actual, measured HTF temperature into the Power Block remains high and relatively constant, while the HTF in the Solar Field cools down, as given by the simulated temperature results.

The actual HTF mass flow rate through a single collector loop in the Solar Field is calculated by dividing the sum of the measured data for volumetric flow rates into each of the four Solar Field quadrants, by the number of loops in the field (156) and using the HTF density at the average design temperature (343°C) to convert to mass flow rate. The obtained actual values can then be compared to simulated results.

Actual data for the HTF temperatures into the superheaters and out of the preheaters, and into and out of the reheaters in each of the two heat-exchanger trains within the Power Block under study, are used to calculate the corresponding specific enthalpy changes from inlet to outlet at each heat exchanger train. This result together with the data for the HTF volumetric flow rates into the superheaters and reheaters in each train, leads to the actual thermal power sent to the Power Block on the HTF side, which can be compared to the simulated value.

Finally, the actual generator output measured in $\mathrm{MW_e}$ at the operating plant is compared to the simulated gross electric power generated.

Figs. 9 and 10 show graphic comparisons of simulated results and actual plant data. All simulated results have been obtained assuming that all receiver tubes are in perfect working condition and keep vacuum, and making use of the specific parameters given in previous sections. The figures show sunny days as well as

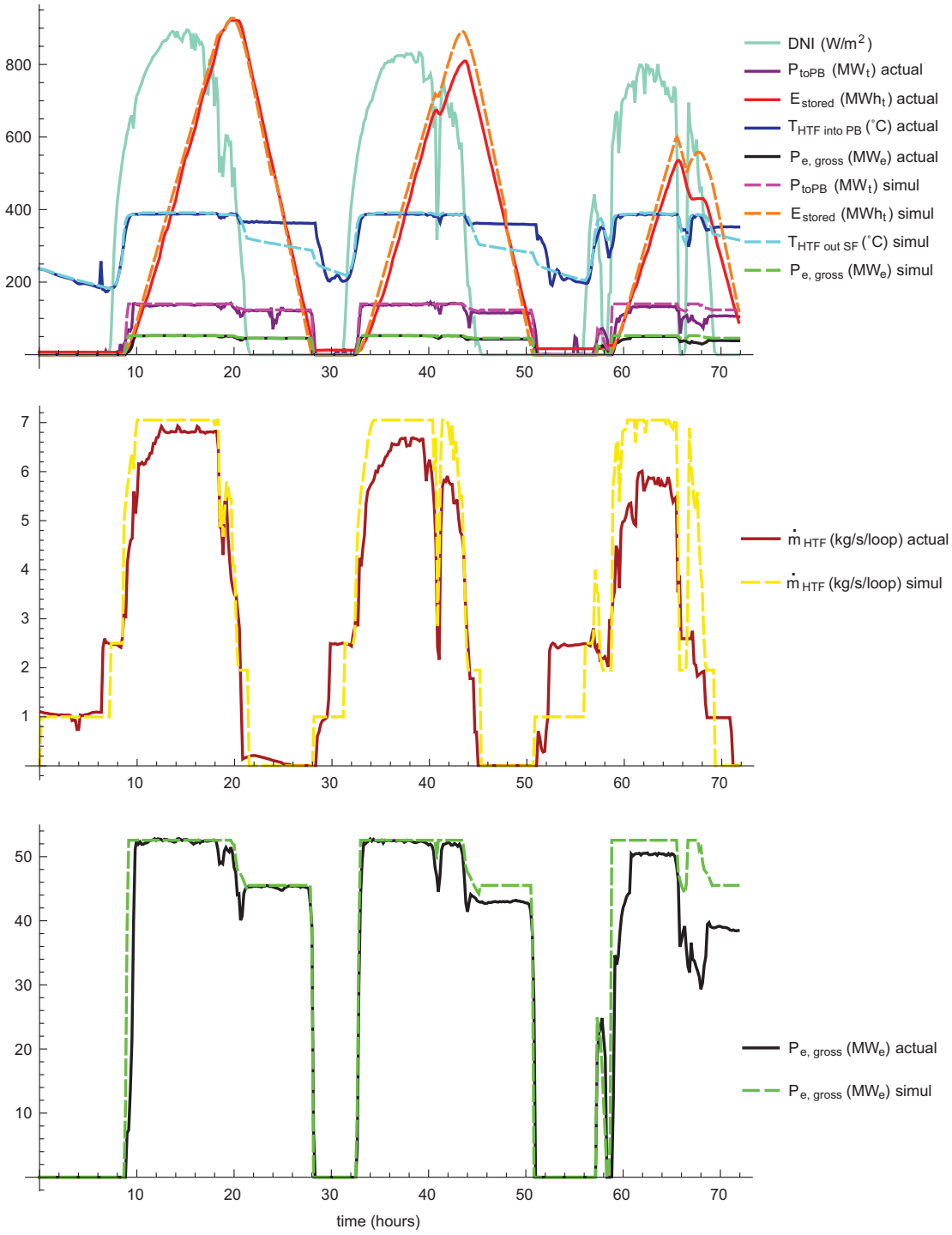

Figure 9: Comparison of actual data and simulated results for three days: 26th, 27th and 28th of June 2010. Ambient temperature during these days was between 13°C and 26°C, wind speed between 0 m/s and 7 m/s and relative humidity between 22 % and 73 %.

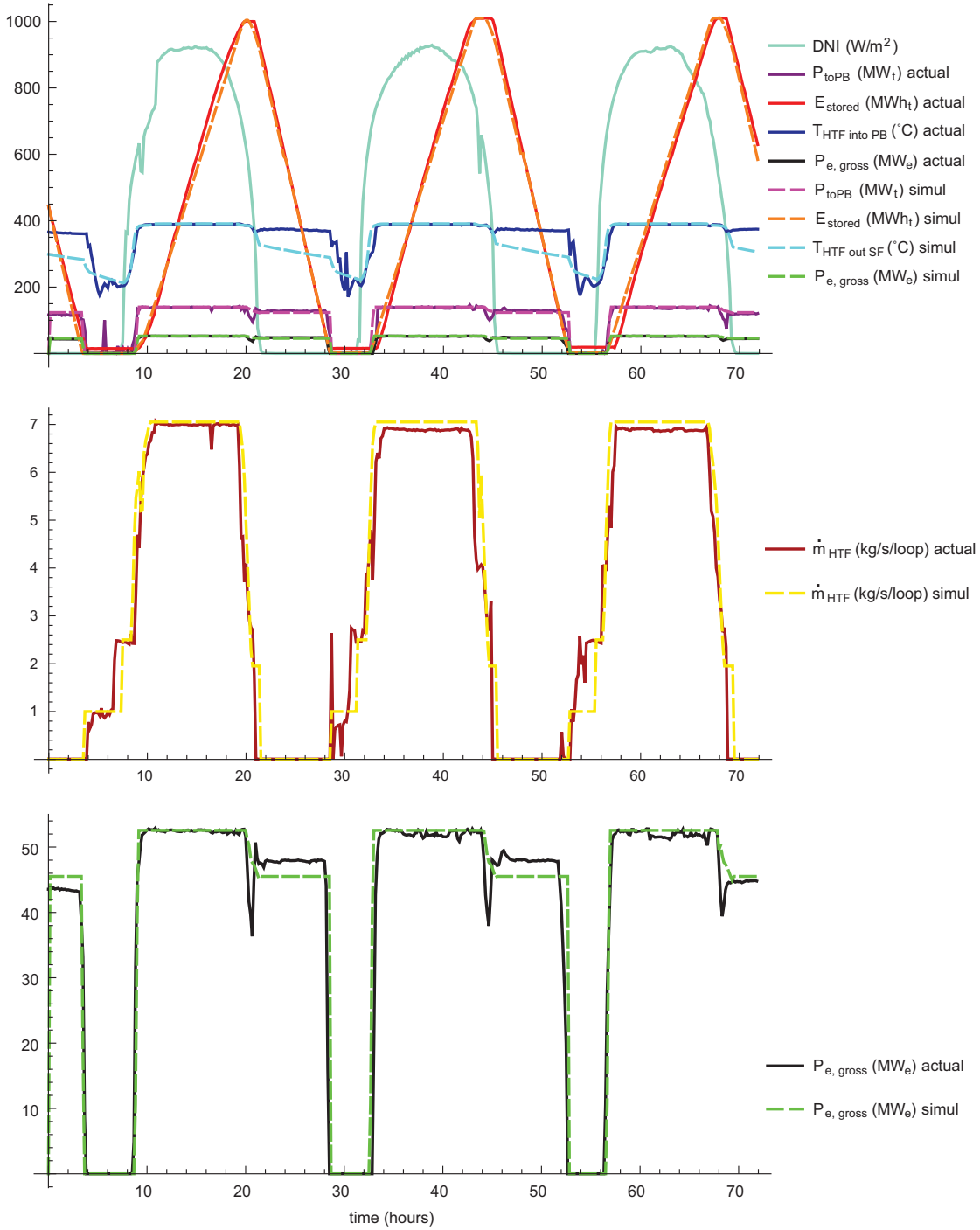

Figure 10: Comparison of actual data and simulated results for three days: 13th, 14th and 15th of July 2010. Ambient temperature during these days was between 13°C and 22°C, wind speed between 0 m/s and 6 m/s and relative humidity between 13 % and 47 %.

days with both slightly and strongly cloudy periods. Note how the simulated HTF temperatures reproduce the actual ones very closely (comparison only applies when no TES discharge takes place) and hence the timing of the actual gross electricity production is well reproduced by the simulated results. The higher simulated production at the end of June 28th in Fig. 9 can be explained by the operator's decision to keep a low HTF flow rate in the Solar Field (and probably de-focus collectors) at around hour 67 in the figure, despite the fact that solar radiation was again high after a strongly cloudy period.

Fig. 11 compares simulated results and actual data for two non-consecutive cloudy days: June 29th (on the left) and July 8th (on the right). Even though the HTF temperature results from the simulation are reasonably close to the actual temperature data, the differences in simulated and actual HTF flow rates in the Solar Field reveal that the operating decisions in the actual plant were different to those made by the modelling algorithm. Between 9 *am* and 10 *am* on June 29th, despite the lack of solar radiation, thermal power is sent to the Power Block in the actual plant, presumably making use of the fossil fuel back up system. This consequently heats up the HTF and results in a peak of generated electricity, as shown in the bottom left plot. The difference in mass flow rates and the decision to stop the circulation of HTF in the Solar Field at around 5 *pm* explain the observed discrepancies between simulated results and actual data towards the end of the day. As for the plots for July 8th on the right hand side of Fig. 11, the operator's decision to keep the HTF mass flow rate low during all daylight hours and to start charging the TES system at around 5 *pm* instead of sending the collected thermal power directly to the Power Block (as in the simulated results), explain the discrepancy between simulated and measured data.

Therefore, if a detailed match between simulated results and actual data is expected, it is essential to have a good knowledge of the typical plant operation strategy. Even if this is the case, deviations can occur, since plants are ultimately run by human decisions during real-time operation.

Fig. 12 shows a comparison of the simulated and actual total daily gross electric energy generated by the plant during the 42 days for which data are available. We find that the agreement between both is remarkably good, with the simulated values being on average 8 % higher than the actual ones.

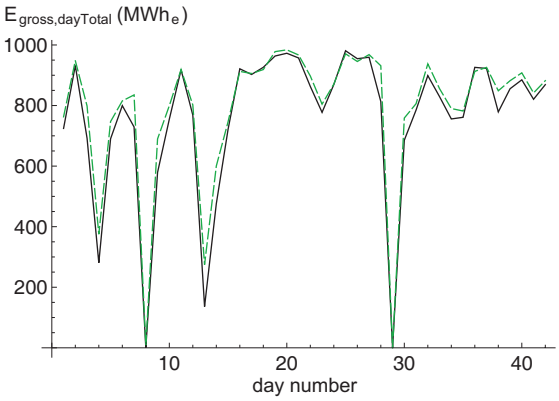

Figure 12: Comparison of simulated (green dashed line) and actual (solid black line) total daily gross electric energy generated by the plant during 42 days, from June 26th to August 6th of 2010.

4. Conclusion and outlook

We have presented a detailed model which simulates the performance of a parabolic trough solar thermal power plant with thermal storage. Details of the algorithm structure and calculations have been presented, and simulated results have been validated against actual data from an operating plant in Spain with excellent agreement. This report is one of the first publications to include actual data from a trough plant with TES system in an attempt to test the accuracy of performance modelling techniques.

The simulation algorithm is flexible and can be generalised to reproduce the performance of any trough plant of choice, since component specifications and particular equations can be easily adjusted to the characteristics of a new project.

We point out the need to consider the actual plant's operation philosophy in order to match the decisions taken by the simulation algorithm to the real ones during operation. This is essential if accurate and detailed results are to be obtained on a daily or hourly basis.

Additionally, the model can be employed as a useful tool to define the design of a project, as well as to assist in the search for an optimised operation strategy.

It would be desirable to carry out a more extended comparison of the simulation results to the actual plant data considering periods within all seasons of the year. However, only summer data were available for the purpose of this paper.

Work is currently in progress to develop a less simplified Power Block model which takes into consideration the fact that meteorological conditions affect the

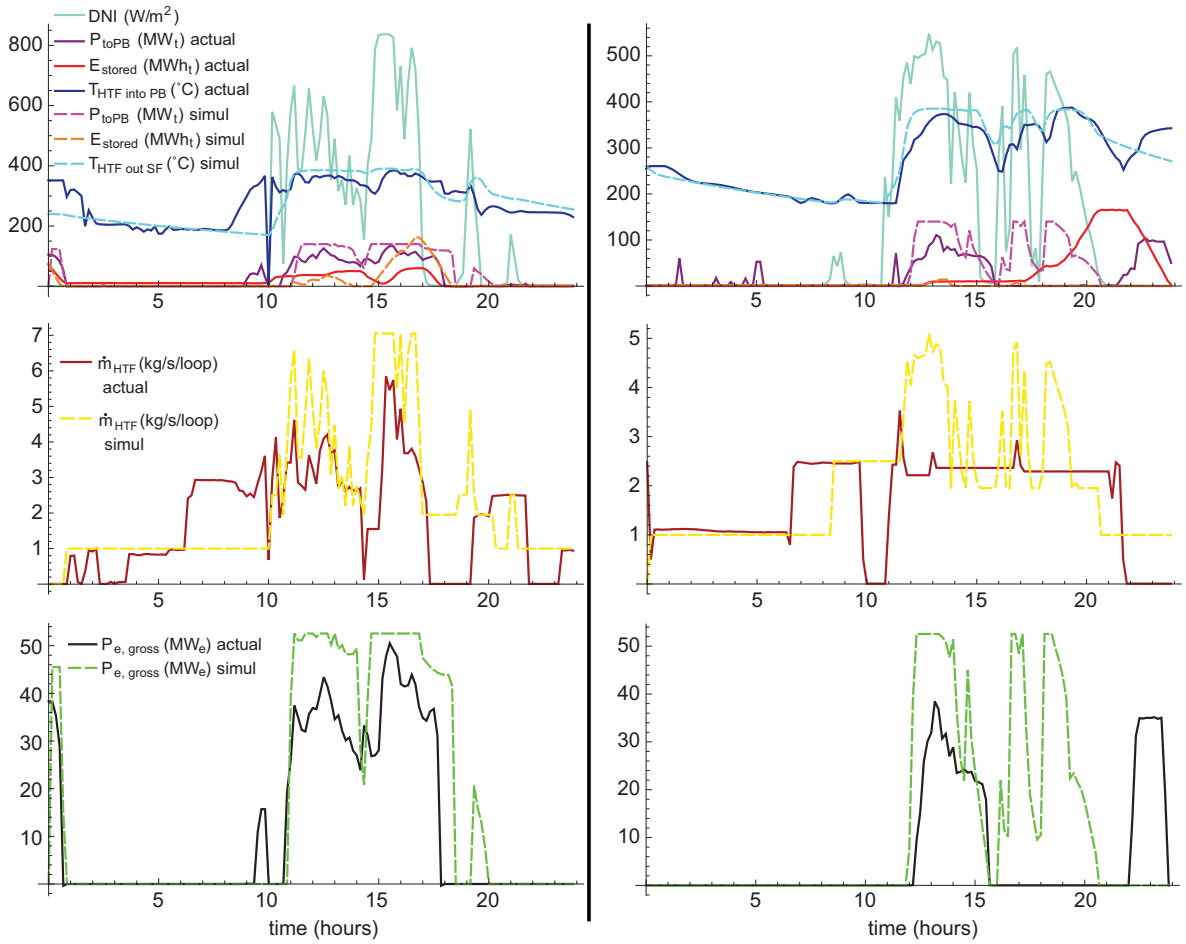

Figure 11: Comparison of actual data and simulated results for June 29th (left) and July 8th (right), 2010. The legend is shared for plots on the left and right hand sides. Note that the zero reading for the actual HTF temperature at 10 *am* on June 29th was caused by a technical fault.

Power Block performance substantially. We estimate that the gross electrical power generated could vary around $2 - 3\,\%$ if we consider the ranges of ambient temperature and relative humidity corresponding to the results shown in section 3.3. The HTF temperature out of the Power Block heat-exchanger trains and into the Solar Field is also affected by ambient conditions, so that we can expect to better reproduce the actual plant data making use of a more detailed Power Block model.

Acknowledgements

The authors wish to acknowledge useful discussions with the rest of the personnel at Initec-Energía during the initial stages of this work. We are indebted to Initec-Energía and the ACS group for funding this work and providing access to operating-plant data.

References

Blair, N., Mehos, M., Christensen, C., 2008a. Modeling photovoltaic and concentrating solar power trough performance, cost and financing with the Solar Advisor Model. NREL CP-670-42922, 1–7.

Blair, N., Mehos, M., Christensen, C., 2008b. Sensitivity of concentrating solar power trough performance, cost, and financing with the Solar Advisor Model. NREL CD-550-42709, 1–8.

Bradford, T., 2006. Solar revolution: the economic transformation of the global energy industry. MIT Press.

Burkholder, F., Kutscher, C., 2008a. Heat-Loss Testing of Schott's 2008 PTR70 Parabolic Trough Receiver. NREL TP-550-42394, 1–54.

Burkholder, F., Kutscher, C., 2008b. Heat-Loss Testing of Solel's UVAC3 Parabolic Trough Receiver. NREL TP-550-42394, 1–19.

Castañeda, N., Vázquez, J., Domingo, M., Fernández, A., León, J., 2006. Sener parabolic trough collector design and testing. SolarPACES 2006 Conference, Seville, Spain.

CIEMAT, 2007. Curso de Sistemas Solares de Concentración.

Dersch, J., Hennecke, K., Quaschning, V., 2008. Greenius - A simulation tool for renewable energy utilisation. Eurosun 2008 Conference, Lisbon, Portugal.

Fernández-García, A., Zarza, E., Valenzuela, L., Pérez, M., 2010. Parabolic-trough solar collectors and their applications. Renewable and Sustainable Energy Reviews 14, 1695–1721.

Greenius, 2011. Software is available from http://www.f1.htw-berlin.de/studiengang/ut/downloads/greenius/index.html.

Hennecke, K., Dersch, J., Quaschning, V., 2010. Greenius - a simulation tool for renewable energy utilization. SolarPACES 2010 Conference, Perpignan, France.

Ho, C. K., 2008. Software and Codes for Analysis of Concentrating Solar Power Technologies. SANDIA report SAND2008-8053, 1–35.

Ho, C. K., Khalsa, S. S., Kolb, G. J., 2011. Methods for probabilistic modeling of concentrating solar power plants. Solar Energy 85, 669–675.

Jones, S. A., Pitz-Paal, R., Schwarzboezl, P., Blair, N., Cable, R., 2001. TRNSYS modeling of the SEGS VI parabolic trough Solar Electric Generating System. Proceedings of ASME International Solar Energy Conference Solar Forum.

Kolb, G. J., 2011. Personal communication. The code is available from Sandia National Laboratories, U.S.

Lamm, L. O., 1981. A New Analytic Expression for the Equation of Time. Solar Energy 26, 465.

Larrain, T., Escobar, R., Vergara, J., 2010. Performance model to assist solar thermal power plant siting in northern Chile based on back up fuel consumption. Renewable Energy 35, 1632–1643.

Lippke, F., 1995. Simulation of the Part-Load Behavior of a 30 MWe SEGS Plant. SANDIA report SAND95-1293.

Montes, M. J., Abanades, A., Martinez-Val, J. M., 2009. Performance of a direct steam generation solar thermal power plant for electricity production as a function of the solar multiple. Solar Energy 83, 679–689.

Patnode, A. M., 2006. Simulation and performance evaluation of parabolic trough solar power plants. Ph.D. thesis, University of Wisconsin-Madison. Department of Mechanical Engineering.

Price, H., 2003. A parabolic trough solar power plant simulation model. NREL CP-550-33209, 1–9.

Price, H. W., Svoboda, P., Kearney, D., 1995. Validation of the FLAGSOL parabolic trough solar power plant performance model. NREL TP-471-7297, 1–6.

Rolim, M. M., Fraidenraich, N., Tiba, C., 2009. Analytic modeling of solar power plant with parabolic linear collectors. Solar Energy 83, 126–1339.

SAM, 2011. SAM software is available from: https://www.nrel.gov/analysis/sam/.

Stine, W. B., Geyer, M., 2001. Power From The Sun. Online book, J. T. Lyle Center for Regenerative Studies, California State Polytechnic University, Pomona., http://www.powerfromthesun.net/.

Stoddard, M. C., Faas, S. E., Chiang, C. J., Dirks, J. A., 1987. SOLERGY - A Computer Code for Calculating the Annual Energy from Central Receiver Power Plants. SANDIA report SAND86-8060.

Wagner, M. J., Blair, N., Dobos, A., 2010. A detailed physical trough model for NREL's Solar Advisor Model. NREL CP-5500-49368, 1–8.

Wilcox, S., Marion, W., 2008. Users Manual for TMY3 Data Sets. NREL TP-581-43156, 1–8.